

# The giant radio galaxy 8C 0821+695 and its environment

L. Lara<sup>1</sup>, K.-H. Mack<sup>2,3</sup>, M. Lacy<sup>4</sup>, U. Klein<sup>3</sup>, W.D. Cotton<sup>5,6</sup>, L. Feretti<sup>2</sup>, G. Giovannini<sup>2,7</sup>, and M. Murgia<sup>2,8</sup>

<sup>1</sup> Instituto de Astrofísica de Andalucía (CSIC), Apdo. 3004, 18080 Granada, Spain

<sup>2</sup> Istituto di Radioastronomia (CNR), Via P. Gobetti 101, I-40129 Bologna, Italy

<sup>3</sup> Radioastronomisches Institut der Universität Bonn, Auf dem Hügel 71, D-53121 Bonn, Germany

<sup>4</sup> IGPP, L-413, Lawrence Livermore National Laboratory, Livermore, CA 94550, USA

<sup>5</sup> National Radio Astronomy Observatory, 520 Edgemont Road, Charlottesville, VA 22903-2475, USA

<sup>6</sup> Sterrewacht Leiden, Niels Bohrweg 2, 2300-RA Leiden, The Netherlands

<sup>7</sup> Dipartimento di Fisica, Università di Bologna, Via B. Pichat 6/2, I-40127 Bologna, Italy

<sup>8</sup> Dipartimento di Astronomia, Università di Bologna, Via Ranzani 2, I-40127 Bologna, Italy

Received / Accepted

**Abstract.** We present new VLA and Effelsberg observations of the radio galaxy 8C 0821+695. We have obtained detailed images in total intensity and polarization of this 2 Mpc sized giant. The magnetic field has a configuration predominantly parallel to the source main axis. We observe Faraday rotation at low frequencies, most probably produced by an ionized medium external to the radio source. The spectral index distribution is that typical of FR II radio galaxies, with spectral indices gradually steepening from the source extremes towards the core. Modeling the spectrum in the lobes using standard synchrotron loss models yields the spectral age of the source and the mean velocity of the jet-head with respect to the lobe material. The existence of a possible backflow in the lobe is considered to relate spectral with dynamical determinations of the age and the velocity with respect to the external medium. Through a very simple model, we obtain a physical characterization of the jets and the external medium in which the radio galaxy expands. The results in 8C 0821+695 are consistent with a relativistic jet nourishing the lobes which expand in a hot, low density halo. We infer a deceleration of the source expansion velocity which we explain through a progressive increase in the hot-spot size.

**Key words:** galaxies: individuals (8C 0821+695) galaxies: active – intergalactic medium – radio continuum: galaxies

## 1. Introduction

Giant Radio Galaxies (GRGs) constitute an unusual class of radio sources with projected linear sizes larger than 1

Mpc<sup>1</sup>. These objects, although giant in size, do not stand out in luminosity, most of them being of low surface-brightness (Subrahmanyam et al. 1996). Moreover, the enormous size of GRGs sometimes hampers the identification of emission from two distant lobes as part of an individual object (e.g. B2 1358+305; Parma et al. 1996). Probably, these are the reasons why to date there are only about 50 known GRGs (Ishwara-Chandra & Saikia 1999; Schoenmakers et al. 2000a). Only recently, radio surveys like the Northern VLA Sky Survey (NVSS; Condon et al. 1998) or the Westerbork Northern Sky Survey (WENSS; Rengelink et al. 1997) allow sensitive searches of GRGs with adequate angular resolution.

Two basic scenarios have been envisaged to explain the outstanding sizes of GRGs. First, their lobes could be fed by extremely powerful central engines which would endow the jets with the necessary thrust to bore their long way through the ambient medium. Second, GRGs could be normal radio sources evolving in very low-density environments offering little resistance to the expansion of the jets. While the first possibility requires the existence of prominent cores and hot-spots, which are not always observed (Ishwara-Chandra & Saikia 1999), the second possibility is supported by the high degree of polarization found in GRGs also at low frequencies (Willis & O’Dea 1990) and seems to be the most plausible scenario in most cases (Mack et al. 1997b). It seems that the expansion of a radio galaxy in a low density environment during a time long enough to allow reaching Mpc sizes, rather than higher than usual radio powers or expansion velocities, are the two basic ingredients to build up the GRG population (Schoenmakers et al. 2000b).

GRGs are located in regions hardly accessible via direct observations: they do not reside in rich galaxy clus-

<sup>1</sup> We assume  $H_0=75 \text{ km s}^{-1} \text{ Mpc}^{-1}$  and  $q_0 = 0.5$  throughout this paper.

ters (Subrahmanyan et al. 1996) and the X-ray emission around their host galaxies is usually weak (Mack et al. 1997a). However, information about the ambient medium at very large distances from the host galaxies can still be gained through the study of their radio properties. Most GRGs probe the intergalactic medium (IGM) providing information about the density of matter outside galactic halos, adding important observational constraints to current cosmological models (Begelman & Cioffi 1989; Nath 1995).

We discuss in this paper new observations of the GRG 8C 0821+695, a Fanaroff-Riley type II (Fanaroff & Riley 1974). It is optically identified with a faint  $M_R \sim 22.2$  galaxy at a redshift of 0.538 (Lacy et al. 1993). Its high redshift, compared to other GRGs, renders 8C 0821+695 a very interesting object since it provides information on the external environment at large cosmological distances. No X-ray source coincident with the radio source is found in the Bright Point Source catalogue from the ROSAT All Sky Survey. At the distance of 8C 0821+695, one arcsecond corresponds to 4.9 kpc.

## 2. Observations and data analysis

We observed 8C 0821+695 with the VLA in the framework of a complete sample of large angular size radio sources selected from the NVSS (see Lara et al. 1999 for a sample description), and with the 100-m Effelsberg telescope. We also incorporate for the discussion maps from the NVSS and WENSS, and maps presented by Lacy et al. (1993). The data have been calibrated according to the scale of Baars et al. (1977).

### 2.1. WENSS and NVSS maps

8C 0821+695 appears as a straight  $\sim 7'$  long FR II radio source in the NVSS and the WENSS maps, with its main axis at a position angle (P.A.) of  $11^\circ$ , measured north through east.

The WENSS map (Fig. 1a), at a frequency of 327 MHz and an angular resolution of  $57''.7 \times 54''.0$ , presents two prominent lobes (N and S) connected by a continuous bridge of emission, although the position of the core is not evident at all.

The NVSS map (Fig. 1b), made at a frequency of 1400 MHz and an angular resolution of  $45''$ , shows a prominent central core straddling the two radio lobes. The N-lobe has higher surface brightness than the S-lobe. The mean fractional polarization ( $p_m$ ) at 1400 MHz is  $p_m=23\%$  in the N-lobe and  $p_m=26\%$  in the S-lobe, while the core is unpolarized. The E-vectors have a similar and rather uniform orientation in the N- and S-lobes, oblique to the source main axis.

### 2.2. Effelsberg observations

We observed 8C 0821+695 with the 100-m Effelsberg telescope at 10.6 GHz (Tab. 1) in order to obtain information about the morphology and polarization properties at high frequencies. The observational and data reduction procedures were those detailed by Gregorini et al. (1992). The maps were CLEANed as described by Klein & Mack (1995). We made 40 coverages resulting –after combining– in a final noise level of 0.5 mJy/beam in total power and 0.1 mJy/beam in the polarized channels. The polarization maps were corrected for the non-Gaussian noise distribution of the polarized intensity, as described by Wardle & Kronberg (1974). This is of particular importance in case of polarized low-brightness regions, e.g. in extended radio lobes.

The 10.6 GHz map (Fig. 1c), with an angular resolution of  $69''$ , shows three components corresponding to the core and the two lobes. The superimposed vectors represent the electrical fields. Since at this high frequency Faraday effects are most probably negligible, a rotation by  $90^\circ$  immediately yields the direction of the projected magnetic field. It is oriented predominantly parallel to the source main axis. The degree of polarization at this frequency is 26% in both lobes.

We also observed 8C 0821+695 with the 100-m telescope at 4850 MHz. After combination of 10 coverages we reached the confusion limit of 0.6 mJy/beam in total intensity, while the noise level was 0.1 mJy/beam in the polarization channels. Because of the large beam size ( $143''$ ), this map does not reveal any additional morphological details, so we do not need to display it here. The degree of polarization derived from the Effelsberg map at 4850 MHz is 19% in the N- and S-lobes.

### 2.3. VLA observations

We made continuum observations of 8C 0821+695 with the VLA in the B- and C-configurations at 1425 and 4860 MHz in dual polarization (see Tab. 1). The interferometric phases were calibrated with the nearby source J0903+679, except during 4860 MHz observations with the B-array, for which J0841+708 was used as phase calibrator. The radio

**Table 1.** Observations of 8C 0821+695

Instrument	$\nu$ (MHz)	$\Delta\nu$ (MHz)	Duration (min)	Date
NVSS	1400	100	–	23 Nov 93
WENSS	327	5	–	–
VLA-C	1425	50	10	19 Feb 96
	4860	100	10	19 Feb 96
VLA-B	1425	50	10	19 Nov 95
	4860	100	10	25 May 97
Effelsberg	10550	300	–	28 Aug 94
	4850	500	–	27 Feb 98

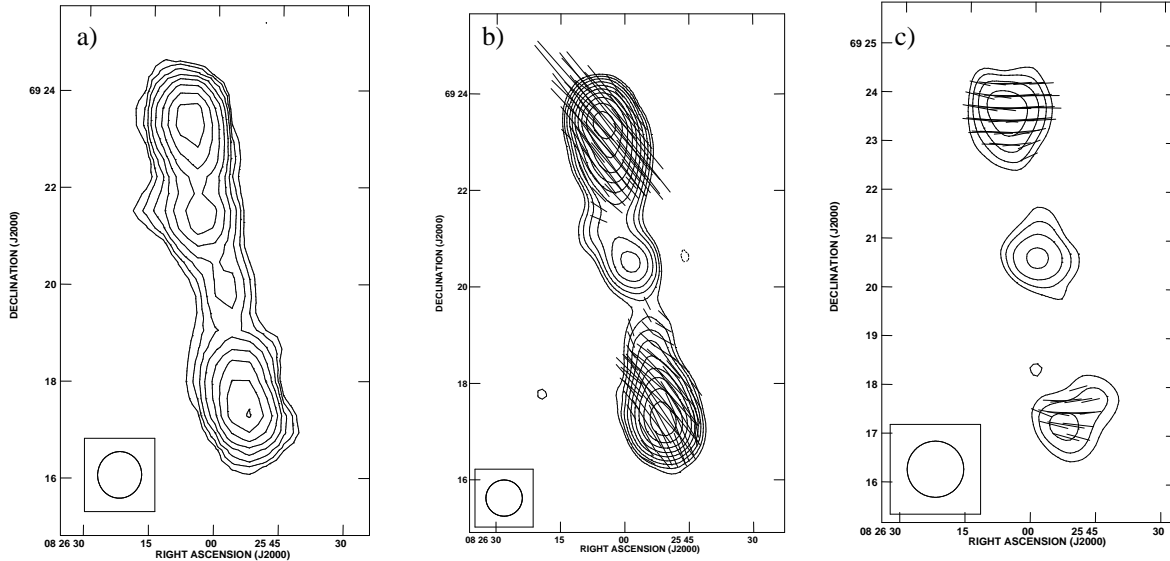


**Fig. 1.** Low resolution maps of 8C 0821+695 from **a)** WENSS (327 MHz), **b)** NVSS (1400 MHz) and **c)** Effelsberg observations (10.6 GHz). Contours are spaced by factors of  $\sqrt{2}$  in brightness, with the lowest at 3 times the rms noise level. The superimposed vectors represent the polarization position angle (E-vector), with lengths proportional to the amount of polarization. From left to right, we list below the rms noise level, the equivalence of  $1''$  length in polarized intensity and the Gaussian beam used in convolution: rms = 3.3, 0.45 and 0.5 mJy beam $^{-1}$ ;  $1'' = 33$  and  $20 \mu\text{Jy beam}^{-1}$ ; Beam =  $57''.7 \times 54''.0$  P.A.  $0^\circ$ ,  $45'' \times 45''$  and  $69'' \times 69''$ .

sources 3C286 and 3C48 served as primary flux density calibrators. Data from the B and C arrays were combined in order to take advantage of the higher B-array resolution and of the higher C-array sensitivity to extended emission. The calibration and mapping of the data were carried out with the NRAO AIPS package. Maps at 4860 MHz had to be corrected from primary beam attenuation. In addition, correction for the non-Gaussian noise distribution in the polarized intensity map was applied.

The VLA map at 1425 MHz shows a well defined compact core, and two lobes of extended emission (Fig. 2a). The N-lobe is dominated by a compact component, suggesting the existence of a faint hot-spot at the end of the jet, while a similar feature is not observed in the S-lobe. The polarized emission of 8C 0821+695 at 1425 MHz comes predominantly from this hot-spot in the N-lobe. At this position, the degree of polarization is 30%. It is 20% in the rest of the N-lobe and 25% in the S-lobe. As in the NVSS map, the electric vectors are inclined with respect to the source main axis, probably due to Faraday rotation.

The VLA map of 8C 0821+695 at 4860 MHz is displayed in Fig. 2b. At this frequency, the core is the most prominent feature. The hot-spot in the N-lobe appears at the end of an elongated structure aligned with the radio axis. The N-lobe shows clear oscillations in its ridge line that are reminiscent of the “dentist drill” model which as-

sumes a jitter of the jet-head with time (Scheuer 1982). On the other hand, the S-lobe appears much more “relaxed” and without a strong hot-spot. We measure a total source length of 6'.95 from Fig. 2b, which corresponds to a projected linear size of 2 Mpc. The north-to-south arm ratio is 0.89.

The polarized emission of 8C 0821+695 at 4860 MHz is again dominated by the N-lobe hot-spot, where we measure a mean degree of polarization of 22%, reaching 26% in the brightest peak. E-vectors are predominantly oriented perpendicularly to the source main axis. We do not detect significant polarization in the S lobe at this frequency and resolution.

Our highest resolution observations (VLA B-array at 4860 GHz) provide the following coordinates for the compact core of 8C 0821+695 (J2000.0): RA =  $08^h 25^m 59^s.770$ , DEC =  $+69^\circ 20' 38''.59$ , fully consistent with the position of the host galaxy.

### 3. Results

#### 3.1. Rotation Measure and depolarization

We have estimated the Rotation Measure ( $RM$ ) over the two radio lobes of 8C 0821+695. To do that, we convolved the NVSS 1400 MHz and the VLA 4860 MHz polarization maps to the beam of the Effelsberg 10.6 GHz map

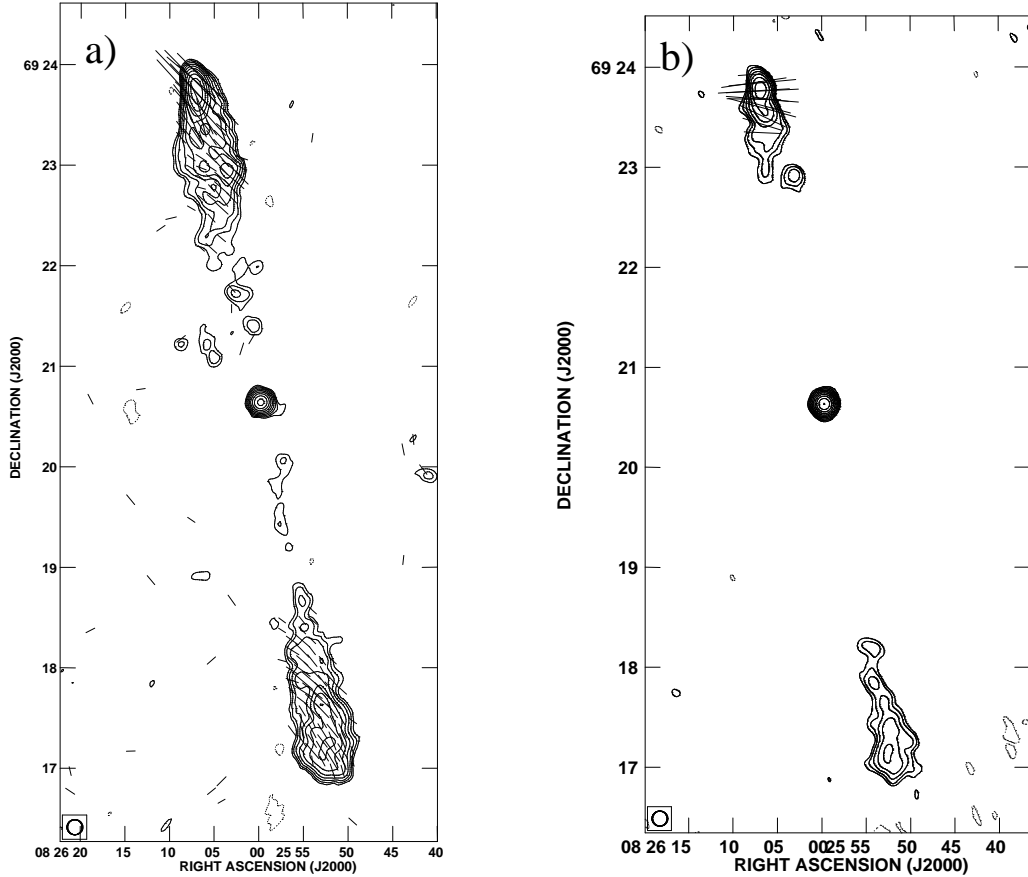


**Fig. 2.** a-b VLA B+C-array maps of 8C 0821+695 at 1425 (left) and 4860 MHz (right). Vectors represent the polarization position angle (E-vector), with length proportional to the amount of polarization ( $1''$  corresponds to  $35 \mu\text{Jy beam}^{-1}$  on the 1425 MHz map and to  $12.5 \mu\text{Jy beam}^{-1}$  on the 4860 MHz map). Contours are spaced by factors of  $\sqrt{2}$  in brightness, with the lowest at 3 times the rms level (rms = 0.13 and 0.1 mJy beam $^{-1}$ , respectively). The Gaussian beam size is  $9'' \times 9''$  in both maps.

(a circular Gaussian beam of  $69''$  FWHM), and applied the AIPS task RM. Although the convolution of the VLA map with such a large beam is in general not advisable, in this case the orientation of the polarization vectors was not seriously affected. We did not use the Effelsberg 4850 MHz map because of its too low angular resolution, which would prevent us from finding any possible structure in the  $RM$  distribution. Even so, we obtain a rather uniform  $RM$  over the two lobes of 8C 0821+695, with an average value of  $-20 \text{ rad m}^{-2}$ .

The uniform and similar distributions of the electric field P.A. and of the  $RM$  over the two lobes suggest that the contribution of the radio source to the observed  $RM$  is negligible. Moreover, the mean galactic  $RM$  at the position of 8C 0821+695 (galactic coordinates  $l = 145^\circ.7$  and  $b = 33^\circ.54$ ) lies between  $-30 \text{ rad m}^{-2}$  and  $0 \text{ rad m}^{-2}$  (Simard-Normandin & Kronberg 1980), consistent with our observed value. We thus conclude that the observed

Faraday rotation is most plausibly of galactic origin, although a small local halo contribution between  $-20$  to  $10 \text{ rad m}^{-2}$  cannot be excluded.

The fractional polarizations derived at different frequencies are essentially consistent with the lack of depolarization at low frequencies. This is clearly derived from the comparison of the low resolution data (10.6 and 5 GHz Effelsberg data and 1.4 GHz data from NVSS), taking into account that the 5 GHz data have a much larger beam and therefore are likely to suffer from beam depolarization. The higher resolution VLA data show that the two lobes are still highly polarized at 1.4 GHz, in agreement with the presence of a magnetic field ordered on the restoring beam scale. We ascribe the lack of detected polarization in the S-lobe at 5 GHz, with  $9''$  resolution, to the lower sensitivity of this image to extended structure.

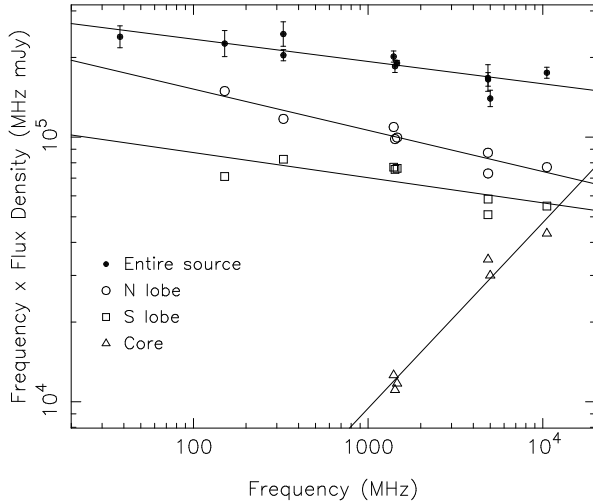


**Fig. 3.** Radio spectrum of 8C 0821+695 and its components. See Table 2 for numerical values and their references.

### 3.2. The broad-band radio-spectrum of 8C 0821+695

We have compiled all available flux density measurements on 8C 0821+695 and have plotted them as a function of frequency giving values, when possible, for the whole source, the two lobes and the core separately (Tab. 2; Fig. 3). We have obtained the spectral index  $\alpha$  (defined so that the flux density  $S \propto \nu^{-\alpha}$ ) of the different components from linear fits to the data:  $\alpha_N = 1.15 \pm 0.02$ ;  $\alpha_S = 1.10 \pm 0.04$ . On the other hand, the core shows a flat spectrum with a mean  $\alpha = 0.30 \pm 0.07$ .

In order to study the dependence of the spectral properties of 8C 0821+695 with frequency and distance from the core, we have made three low resolution spectral in-

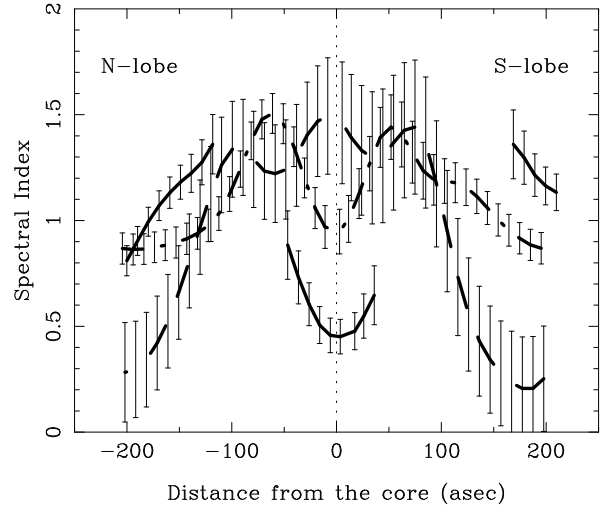


**Fig. 4.** Profiles of the spectral index of 8C 0821+695 along its main axis with an angular resolution of  $69''$ . - - -: spectral index between 151 and 327 MHz; - · - · -: spectral index between 327 and 1400 MHz; —: spectral index between 1400 and 10550 MHz.

**Table 2.** Flux density of 8C 0821+695

Freq. (MHz)	Integrated flux density of				Ref.
	Entire source (mJy)	N lobe (mJy)	S lobe (mJy)	Core (mJy)	
38	6300 ± 600	—	—	—	(1)
151	1495 ± 170	989	470	—	(2)
327	750 ± 80	—	—	—	(3)
327	623 ± 31	358	252	—	(4)
1400	144 ± 7	78	55	9	(5)
1425	130 ± 7	69	53	8	(6)
1465	130 ± 3	68	52	8	(2)
4850	34.5 ± 4	18	10.5	—	(7)
4860	34 ± 2	15	12	7	(6)
5000	28 ± 2	—	—	6	(2)
10550	16.6 ± 0.8	7.3	5.2	4.1	(7)

- (1) Rees 1990; (2) Lacy et al. 1993; (3) Wieringa 1991;  
(4) WENSS; (5) NVSS; (6) This work, VLA;  
(7) This work, Effelsberg

dex maps using the 10.6 GHz Effelsberg, the 1400 MHz NVSS, the 327 MHz WENSS and the 151 MHz CLFST map by Lacy et al. (1993). To construct the  $\alpha$ -maps, all total intensity maps were convolved to a circular beam of  $69''$ , and then were registered to the nominal position of the core. Figure 4 displays spectral index profiles along the main radio axis for the three frequency intervals, with plotted  $1-\sigma$  errors deduced taking into account the rms noise level of each image and the uncertainties in their flux density scales. The core shows up as a flattening of the spectrum at the center of the higher frequency profiles. In both lobes we find an overall steepening of the spectrum from the extremes towards the compact core, a behaviour typical of FR II radio sources. In addition, the steepening of the spectrum with increasing frequency is also evident from this plot. The spectrum at low frequencies is rather flat in the source extremes. This result is expected since these regions are dominated by the flat spectrum hot-spot like regions and is consistent with the injection spectral index derived in Sect. 3.4.

To study in detail the spectral index distribution over 8C 0821+695 we have made a high-resolution  $\alpha$ -map registering our VLA maps at 1425 and 4860 MHz to the position of the core and performing a pixel-by-pixel evaluation of the spectral index between these two frequencies (Fig. 5). We find the same general trends observed at lower resolutions, but convolved with a now evident structure in the  $\alpha$ -distribution. The core shows a flat spectrum between these two frequencies. The lobes present similar spectral indices, although the N-lobe hints at a slightly steeper spectrum which, if real, would indicate a more efficient energy dissipation in this region.

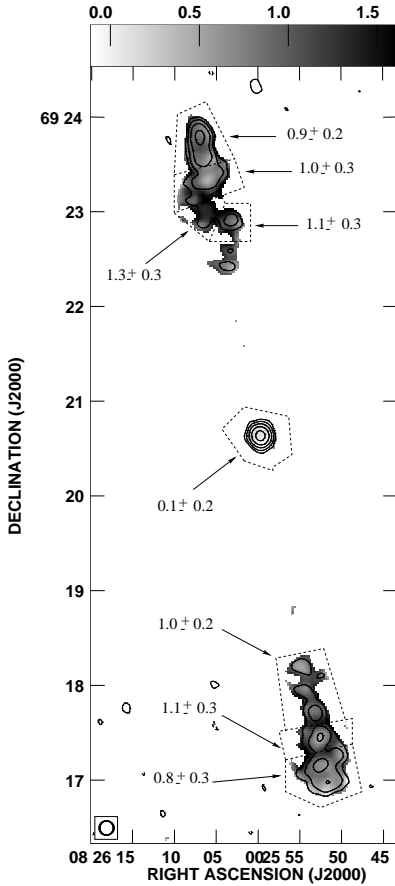


**Fig. 5.** Spectral index, in grey-scale, of 8C 0821+695 between 4860 and 1425 MHz, with an angular resolution of  $9'' \times 9''$ . The contours represent total intensity at 5 GHz to facilitate the identification of emission regions in the radio source with spectral trends. Numerical values of the mean spectral index over selected regions are indicated for clarity.

### 3.3. Physical parameters of 8C 0821+695

We have measured the FWHM and the surface brightness at several positions on the ridge line of 8C 0821+695 by fitting Gaussians to surface brightness profiles taken perpendicular to the source main axis in the high-sensitivity 1400 MHz map by Lacy et al. (1993). The deconvolution of the width and surface brightness was done following Appendix A in Killeen et al. (1986). We used the standard formulae of synchrotron radiation (e.g. Miley 1980) to calculate the minimum energy density  $u_{me}$  at these positions and the corresponding magnetic field  $B_{me}$ , which is approximately the equipartition field. The total pressure is assumed to be that of equipartition between particles and magnetic field,  $P_{eq} = 0.62 u_{me}$ . Besides, the following assumptions were made in the calculations: *i*) the magnetic field is assumed to be random; *ii*) the energy of particles is equally stored in the form of relativistic electrons

and heavy particles; *iii*) lower and upper frequency cut-offs were set to 10 MHz and 100 GHz, respectively; *iv*) the spectral index is 1.1; and *v*) the line-of-sight depth is equal to the deconvolved FWHM. The results are listed in Tab. 3 as a function of the filling factor of the emitting regions  $\eta$ .

### 3.4. Spectral aging

Based on the maps at 151 MHz (Lacy et al. 1993), 327 MHz (WENSS), 1.4 GHz (NVSS), 4.8 GHz (VLA) and 10.4 GHz (Effelsberg), we have performed a spectral aging analysis of 8C 0821+695. We have determined the spectrum at different positions of the source averaging the flux density over selected regions with a beam equivalent area ( $69''$ ) in order to insure independent measurements. Three selected regions were centered on the N-lobe (at the position of the hot-spot and at 711 and 364 kpc from the core) and other three on the S-lobe (at the southern extreme and at 903 and 553 kpc from the core).

We show in Fig. 6 the spectra of the different selected regions and the fits to the data after the application of synchrotron loss models. Left and right panels refer to the N- and S-lobe, respectively. The spectra at the source extremes (top panels) are best fitted by the continuous injection model (CI; Pacholczyk 1970), giving an injection spectral index of  $\alpha_{inj} = 0.4$  for the northern hot-spot and  $\alpha_{inj} = 0.6$  for the southern extreme of the source, in agreement with the low frequency spectral index in Fig. 4. The spectra in these regions show a break at low frequencies ( $\sim 1$  GHz) with a moderate steepening afterwards. However, the flat spectrum of the hot-spots at low frequencies might indicate that the source here is optically thick and any spectral fit in these regions must be taken with caution. Moreover, Meisenheimer et al. (1989) find that low frequency breaks at hot-spots are more likely related to the ratio between the outflow distance and the outflow velocity of the post-shocked material after the Mach disk rather than to synchrotron aging. Thus, we will not use the information of the break frequency at the source extremes to derive synchrotron ages.

Middle panels in Fig. 6 correspond to the spectra taken at 711 kpc (N-Lobe) and 903 kpc (S-Lobe) from the core, respectively. Our data do not allow us to distinguish between the Jaffe-Perola (JP; Jaffe & Perola 1973) or the Kardashev-Pacholczyk (KP; Kardashev 1962, Pacholczyk 1970) synchrotron loss models, both producing equivalent results. An injection spectral index  $\alpha_{inj} = 0.7$  has been found and kept fixed in these fits. The discrepancy between the injection spectral index in the lobes and in the hot-spots is similar to that found in Cygnus A (Carilli et al. 1991), although a physical interpretation of this fact remains unclear. The derived break frequencies are 15 GHz at 711 kpc in the N-lobe and 18 GHz at 903 kpc in the S-lobe.

**Table 3.** Physical parameters for the N- and S- lobes

Distance (kpc)	FWHM (kpc)	Brightness (mJy/beam <sup>a</sup> )	B <sub>me</sub> (η <sup>-2/7</sup> μG)	u <sub>me</sub> (η <sup>-4/7</sup> J m <sup>-3</sup> )	P <sub>eq</sub> (η <sup>-4/7</sup> N m <sup>-2</sup> )
North lobe					
340	85	2.5	3.8	1.4 × 10 <sup>-13</sup>	8.5 × 10 <sup>-14</sup>
480	98	1.9	3.4	1.1 × 10 <sup>-13</sup>	6.7 × 10 <sup>-14</sup>
630	109	4.6	4.3	1.7 × 10 <sup>-13</sup>	1.0 × 10 <sup>-13</sup>
775	104	7.3	4.9	2.3 × 10 <sup>-13</sup>	1.4 × 10 <sup>-13</sup>
923	27	42.6	12.0	1.3 × 10 <sup>-12</sup>	8.2 × 10 <sup>-13</sup>
South lobe					
433	91	0.8	2.7	6.9 × 10 <sup>-14</sup>	4.3 × 10 <sup>-14</sup>
579	85	1.4	3.3	9.9 × 10 <sup>-14</sup>	6.1 × 10 <sup>-14</sup>
726	98	3.1	3.9	1.4 × 10 <sup>-13</sup>	8.9 × 10 <sup>-14</sup>
872	79	6.8	5.2	2.5 × 10 <sup>-13</sup>	1.6 × 10 <sup>-13</sup>
1019	104	8.8	5.2	2.5 × 10 <sup>-13</sup>	1.6 × 10 <sup>-13</sup>

<sup>a</sup> The beam is a circular Gaussian of 15'' × 15''

Bottom panels in Fig. 6 refer to the two regions nearest to the core, at 363 kpc (N-Lobe) and 553 kpc (S-Lobe). Again, fits using KP and JP models are indistinguishable. The break frequency is 1.6 GHz in the N-lobe and 2.2 GHz in the S-lobe. Due to the sharp cut-off, the flux densities at 4.8 and 10 GHz are below the noise level. In the fit we kept  $\alpha_{inj} = 0.7$  as a fixed parameter.

Synchrotron ages were derived from the break frequencies in the lobes using the equation (Carilli et al. 1991):

$$t_{syn} = 1.61 \times 10^3 \frac{\sqrt{B_{eq}}}{B_{eq}^2 + B_{IC}^2} \frac{1}{\sqrt{\nu_B(1+z)}}. \quad (1)$$

The synchrotron age  $t_{syn}$  is given in Myr, the break frequency  $\nu_B$  in GHz and magnetic fields in  $\mu\text{G}$ . For the strength of the equipartition magnetic field  $B_{eq}$  we took the corresponding values from Tab. 3, and a magnetic field equivalent to the Inverse Compton microwave background of  $B_{IC} = 7.7 \mu\text{G}$  ( $B_{IC} = 3.25(1+z)^2$ ). The spectral ages derived from the data are plotted in Fig. 7. The errors in the spectral ages can be derived from the uncertainties of  $B_{eq}$  and  $\nu_B$ ; however, when  $B_{eq} \sim \frac{B_{IC}}{\sqrt{3}}$  (as it is approximately given in our case), the total error is dominated by the uncertainties of the break frequencies. Therefore errors in Fig. 7 depend directly on the errors in the break frequencies which we have estimated considering the 1- $\sigma$  region of allowance in the space of free-parameters in the fits. A weighted least-square fit yields a mean expansion velocity of 0.08 c for both lobes, which represents a measure of the rate of separation of the jet-head from the lobe material. The source spectral age, obtained by extrapolation of the age profiles up to the core, is 42 Myr. We note that the derived expansion velocity is consistent with that obtained assuming a zero age at the hot-spots, supporting the reliability of our spectral fit argument.

## 4. Discussion

### 4.1. The “conical” lobe

In this section we propose a simple scenario of a jet nourishing a radio lobe with the aim of constraining the physical parameters of the jet itself and of the ambient medium surrounding the radio emission. We consider the geometry outlined in Fig. 8 for the jet and the lobe of a radio galaxy, and assume that the external medium is uniform and steady. Relativistic corrections are not taken into account here, since lobe propagation velocities are small compared with the speed of light (eg. Begelman et al. 1984).

In general, the ratio of the advance speed of the emitting body (the jet-head velocity  $v_h$ ) to the sound speed of the unperturbed external region ( $v_s$ ), is related to the angle between the shock front and the velocity direction (the Mach angle  $\Phi$ ), through the equation:

$$\begin{aligned} \sin \Phi &= \frac{v_s}{v_h} \\ &= \frac{1}{v_h} \sqrt{\frac{\gamma P_a}{\rho_a}}, \end{aligned} \quad (2)$$

where  $\gamma$ ,  $P_a$  and  $\rho_a$  are the adiabatic index, the pressure and the mass density of the ambient medium, respectively. The mass density may also be written  $\rho_a = \sigma n_a$ , where  $\sigma$  is the mean atomic weight and  $n_a$  is the number of particles per unit volume. Assuming an ideal gas, the pressure, density and temperature are related through the equation of state  $P_a = n_a k T_a$ , where  $k$  is the Boltzmann’s constant and  $T_a$  is the temperature of the ambient medium. Equation 2 provides a relationship between  $v_h$ , the lobe geometry and the properties of the external medium.

We note that  $v_h$  as given in Eq. 2 corresponds to the advance velocity of the jet-head with respect to the external medium at the time of the observations since it

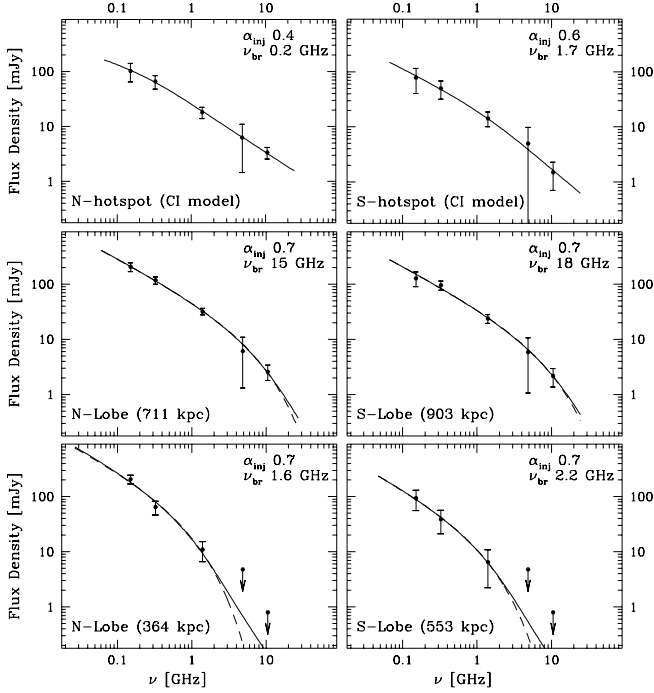


**Fig. 6.** Spectra at different regions of 8C 0821+695. Left and right panels refer to the N- and S-lobe, respectively. Upper panels correspond to the spectra at the source extremes (hot-spots), fitted by CI model. Middle and bottom panels correspond to lobe regions at 711 and 364 kpc (N-lobe), and 903 and 553 kpc (S-lobe) from the core, respectively, where data have been fitted with a KP (continuous line) and JP (dashed line) models. Upper limits in the bottom panels are at the rms noise level of the corresponding maps.

depends only on local conditions measured close to the hot-spot. On the other hand, determinations based on aging arguments (Sect. 3.4) correspond to the jet-head velocity measured with respect to the lobe emitting material and averaged over the whole life of the radio source ( $\langle v'_h \rangle$ ). Even if all our assumptions are correct, these two estimations of the advance velocity,  $v_h$  and  $\langle v'_h \rangle$ , may be different *i*) if the backflow  $v_{bf}$  of the lobe material is not negligible or *ii*) if the jet-head is accelerated, so that comparing mean and instantaneous velocities is meaningless. Besides, incorrect assumptions (e.g. deviations from minimum energy conditions, a break frequency distribution not related to the separation velocity, wrong estimations of the external physical parameters, etc.) may lead to differing results (see Carilli et al. 1991 for a detailed discussion). In the following we will consider that all our assumptions are reasonably good approximations to the real physical situation.

The absence or presence of diffuse extended tails of emission perpendicular to the source axis provide informa-

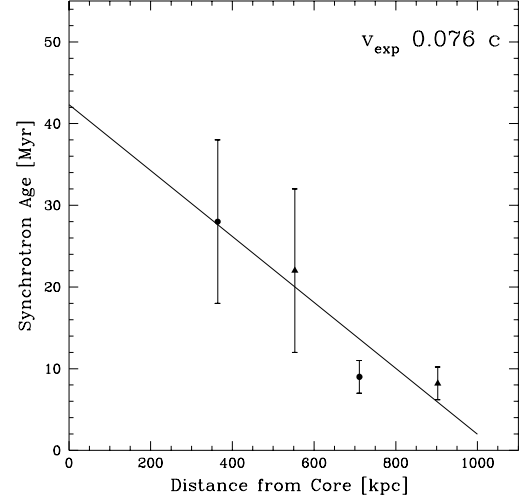


**Fig. 7.** Spectral ages as a function of core distance in 8C 0821+695. Filled dots refer to the N-lobe; triangles to the S-lobe. A mean expansion velocity of 0.08 c is derived from a linear fit to the data. A source spectral age of 42 Myrs is derived from the extrapolation at zero distance.

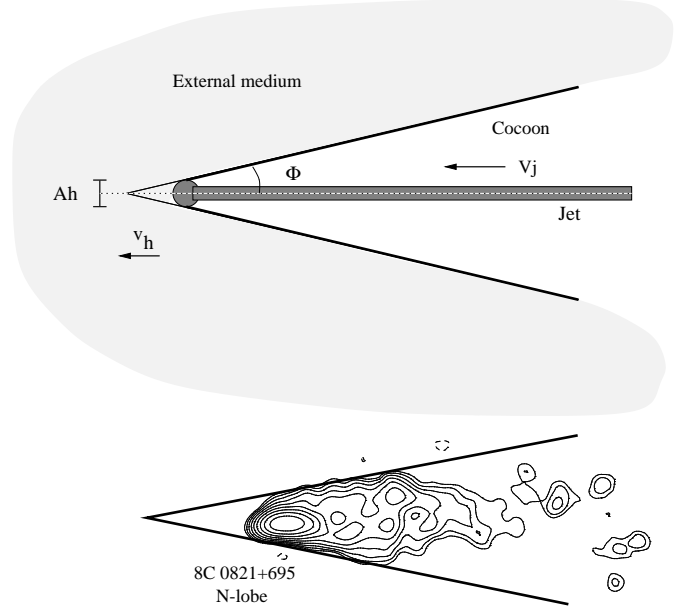


**Fig. 8.** Top: schematic representation of the jet and the lobe of a radio galaxy expanding in an uniform and homogeneous environment. Bottom: translation of this scheme to the northern lobe of 8C 0821+695.

tion of how important the backflow of lobe material is. In general, we will consider that the mean backflow velocity is a factor  $\epsilon$  of the mean advance velocity of the jet-head with respect to the external medium, i.e.  $\langle v_{bf} \rangle = \epsilon \langle v_h \rangle$ , so that the velocity of the head with respect to the lobe



$\langle v'_h \rangle = (1 + \epsilon)\langle v_h \rangle$ . Similarly, the spectral age is related to the dynamical age of the source as  $t = (1 + \epsilon)t_{syn}$ . Moreover, we can assume a constant jet-head deceleration and determine the initial head velocity  $v_{hi}$  as

$$v_{hi} = 2(1 + \epsilon)^{-1}\langle v'_h \rangle - v_h. \quad (3)$$

On the other hand, the balance of the ram pressure of the ambient medium and the thrust of the jet, spread over the cross-sectional area  $A_h$  of the bow shock at the end of the jet is (Begelman & Cioffi 1989):

$$v_h \sim \sqrt{\frac{L_j}{\sigma n_a v_j A_h}}, \quad (4)$$

where  $L_j$  is the total jet power and  $v_j$  is the jet bulk velocity. In an uniform medium and if these two jet parameters were constant with time, a varying  $v_h$  could be obtained through a variation in the contact surface  $A_h$ . We note that a constant  $A_h$  and  $n_a$  decreasing with core distance would lead to  $v_h$  increasing with time, a situation highly unphysical (Loken et al. 1992). Although a combination of both situations might occur leading to a given  $v_h$  evolution, we will neglect density variations for simplicity. Therefore, from Eq. 4, we find a relation between  $v_h$  and  $A_h$  at present and initial conditions:

$$A_h = A_{hi} \left( \frac{v_{hi}}{v_h} \right)^2. \quad (5)$$

This relation translates to an opening angle ( $\theta$ ), defined by the time evolution of the contact surface, given by

$$\tan \theta = \frac{\sqrt{\frac{A_h}{\pi}} \left( 1 - \frac{v_h}{v_{hi}} \right)}{l}, \quad (6)$$

where  $l$  is the total jet length.

#### 4.2. Application to 8C 0821+695

The N-lobe of 8C 0821+695 clearly resembles the simple geometry outlined in Fig. 8, so it seems reasonable to apply the previous analysis to this lobe. Even if we need to make several assumptions and the uncertainties of our results are high, we obtain at least an idea of the order of magnitude of the different parameters, which is the aim of these calculations.

From the VLA maps at 4860 and 1425 MHz (Fig. 2), we measure an angle  $\Phi = 12^\circ$  at the N-lobe (see Fig. 8). However, we note that this value is a lower limit to the true Mach angle since we implicitly assume that the edge of the synchrotron emitting region defines the lobe contact discontinuity, and that this discontinuity is coincident with the bow shock produced by the jet-head advance in the external medium. Such assumption underestimates the true Mach angle, since it implies that the region of shocked external medium between the contact discontinuity and the

bow shock is negligible. Moreover, we assume  $\sigma = 1.4$  amu,  $\gamma = \frac{5}{3}$  and an upper limit of  $T_a = 10^7$  K for the external medium temperature (Barcons et al. 1991).

We have accepted the minimum energy conditions and used the NVSS and WENSS maps to derive the cocoon pressure at low brightness regions in the lobes of 8C 0821+695, far away from the hot-spot; we obtain  $P_c \sim 1.5 \times 10^{-14}$  Nm<sup>-2</sup>. Strictly speaking, this value constitutes an upper limit to the external pressure  $P_a$  since the bridges in FR II radio sources are most probably over-pressured with respect to the surrounding medium (e.g. Subrahmanyan & Saripalli 1993; Nath 1995). However, observations (Subrahmanyan et al. 1996) and models (Kaiser & Alexander 1997) indicate that the lobes of FR II radio galaxies grow in a self-similar way, so that GRGs are expected to have the lowest pressures, being closer to a situation of pressure equilibrium with the outer medium than other FR II radio galaxies. Thus, we can reasonably assume for our calculations that the low-brightness regions in the lobes of 8C 0821+695 provide a good approximation of the ambient gas pressure  $P_a$  (see also Schoenmakers et al. 2000b). In fact, the pressure we obtain is as low as that found at the very periphery of galaxy clusters, confirming that the environment of this giant source is tenuous.

Considering the upper limit temperature of  $10^7$  K for the ambient gas, the particle density resulting from the equation of state is about  $10^2$  m<sup>-3</sup>. This density is consistent with the limit on  $RM$  ( $|RM| \leq 20$  rad m<sup>-2</sup>) if the ambient uniform magnetic field is about  $0.5$   $\mu$ G and the Faraday depth less than 1 Mpc, which are reasonable values since we do not expect a strong field to be distributed over large regions.

From Eq. 2, we obtain  $v_h \sim 5 \times 10^{-3}$  c which, according to our assumptions is an upper limit to the true jet-head velocity. Besides, from spectral aging arguments (Sect. 3.4) we obtained a mean expansion velocity of the head with respect to the lobe material  $\langle v'_h \rangle = 0.08$  c. On the other hand, Lacy et al. (1993) find evidence of a tail at the base of the N-lobe and suggest a backflow speed close to the advance speed of the head. According to that, we will assume  $\epsilon \simeq 1$ , so that  $\langle v_h \rangle \simeq \langle v_{bf} \rangle \simeq 0.04$  c. Using Eq. 3, we estimate an initial jet-head velocity  $v_{hi} \sim 0.075$  c.

The area of the head contact surface  $A_h$  can be derived by fitting an elliptical Gaussian to the northern hot-spot at 5 GHz. We obtain a deconvolved angular diameter of  $\sim 5''$  ( $\sim 25$  kpc). We can then calculate the total power of the jet from Eq. 4, assuming a jet bulk velocity  $v_j \sim c$  (Fernini et al. 1997). We obtain  $L_j = 7.1 \times 10^{37}$  W. Alternatively, we can estimate the total power from the average minimum energy density ( $\bar{u}_{me} = 2.7 \times 10^{-13}$  J m<sup>-3</sup>; Tab. 3), the volume of the source (simplified to a cylinder of 2 Mpc $\times$ 200 kpc) and its dynamical age  $t = 2t_{syn} = 84$  Myr, giving  $L = 9 \times 10^{37}$  W, fully consistent with the previous result.

From Eq. 5, the angular diameter of the jet contact surface at the initial stages of the source is about  $0''.33$ . The increase in the contact surface from this value to the measured one ( $5''$ ) requires an opening angle  $\theta$ , defined by the hot-spot size evolution, of  $0''.7$  (Eq. 6). Thus, a small increase of the hot-spot size with time can naturally explain the deceleration of the jet-head and the difference in the velocity determinations from local and global conditions.

Finally, the radio power of the northern lobe  $L_r$  can be derived from the observed flux density and spectral index:

$$L_r = 4\pi D_L^2 \int_{\nu_1}^{\nu_2} S(\nu) d\nu, \quad (7)$$

where  $D_L$  is the luminosity distance, and  $\nu_1 = 10$  MHz and  $\nu_2 = 100$  GHz are the assumed lower and upper frequency cutoffs. Since  $S(\nu) \propto \nu^{-\alpha}$  and  $\alpha = 1.1$ , we obtain  $L_r = 6.9 \times 10^{35}$  W.  $L_r$  being about two orders of magnitude lower than  $L_j$  would indicate that most of the jet power is devoted to the expansion of the lobe against the external medium. Results are summarized in Table 4.

**Table 4.** 8C 0821+695 and its environment

Ambient density	$n_a$	$\sim 100$	$\text{m}^{-3}$
Ambient pressure	$P_a$	$\sim 1.5 \times 10^{-14}$	$\text{N m}^{-2}$
Present head velocity	$v_h$	$\sim 0.005$	c
Mean head velocity	$\langle v_h \rangle$	$\sim 0.04$	c
Initial head velocity	$v_{hi}$	$\sim 0.075$	c
Spectral Age	$t_{syn}$	$\sim 4.2 \times 10^7$	yr
Dynamical Age	$t$	$\sim 8.4 \times 10^7$	yr
Northern jet Power	$L_j$	$\sim 7 \times 10^{37}$	W
N-lobe radio power	$L_r$	$\sim 7 \times 10^{35}$	W
Opening angle	$\theta$	$\sim 0''.7$	

The S-lobe does not present such a suitable morphology for the application of the previous simple model since the head of the lobe does not have a clear cone-like appearance (see Sect. 2.3). From the observed arm-ratio, we might deduce that the external medium here could be more tenuous than in the northern lobe region.

## 5. Conclusions

We present new radio observations made with the VLA and the 100-m Effelsberg radio telescope, of the GRG 8C 0821+695 at different frequencies and angular resolutions. Our data have been analyzed together with survey and literature data in order to study the details of a high-redshift GRG, and obtain information about the external medium surrounding the radio source.

8C 0821+695 is a straight 2 Mpc long FR II radio source, with a north-to-south arm-ratio of 0.89. The N-lobe contains a hot-spot, responsible for most of the source polarized emission. The S-lobe presents a more relaxed

structure, without a well defined hot-spot. At high frequencies ( $\nu \geq 1400$  MHz) 8C 0821+695 shows a prominent compact core. We have not found any trace of the jets nourishing the lobes.

The spectral index distribution over the lobes of 8C 0821+695 is typical of FR II-type radio galaxies, showing a gradual steepening from the outer ends towards the core. The mean lobe spectral index is  $\alpha = 1.1$ . The core has a flat spectrum with  $\alpha = 0.3$ . Using the available data, we have made a spectral-aging analysis of the source lobes, providing the dependence of the spectral break frequency and the synchrotron age with the distance from the core. We obtain a mean expansion velocity of the jet head with respect to the lobe material of 0.08 c, and a spectral age of 42 Myr. This age determination might be affected by the possible existence of backflow of material in the lobe, being a lower limit to the true age. The age we derive for 8C 0821+695 is of the order of ages estimated for other GRGs (Schoenmakers et al. 2000b).

We have studied the *RM* over the lobes of 8C 0821+695, obtaining a smooth and uniform distribution, which we ascribe to Faraday rotation mostly produced by the Galactic medium. Equipartition conditions have been assumed in order to derive physical parameters of the lobes at different positions, yielding magnetic fields, pressures and energy densities that are consistent with estimated values in other GRGs.

Under very simple assumptions we have estimated physical parameters of the jet and the external medium of 8C 0821+695. We find that the present expansion velocity is significantly lower than the mean expansion velocity even if backflow is allowed, implying the existence of deceleration. We explain this deceleration by an increase of the cross-sectional area of the bow shock at the end of the jet with time. We note that external density estimates in the literature for other GRGs usually consider the contact surface measured at the time of the observations together with mean quantities (like the expansion velocity derived from aging arguments), resulting in external densities lower than the density we obtain. However, our results are still consistent with GRGs evolving in poor density regions.

*Acknowledgements.* We thank the referee Dr. R. Perley for helpful and constructive comments to the paper. The National Radio Astronomy Observatory is a facility of the National Science Foundation operated under cooperative agreement by Associated Universities, Inc. This research has made use of the NASA/IPAC Extragalactic Database (NED) which is operated by the Jet Propulsion Laboratory, California Institute of Technology, under contract with the National Aeronautics and Space Administration. This research is supported in part by the Spanish DGICYT (PB97-1164). KHM was supported by the European Commission, TMR Programme, Research Network Contract ERBFMRXCT96-0034 ‘‘CERES’’. LF, GG and MM acknowledge a partial support by the Italian Ministry for University and Research (MURST) under grant Cofin98-02-32.

## References

- Baars J.M.W., Genzel R., Pauliny-Toth I.I.K., Witzel A., 1977, *A&A*, 61, 99
- Barcons X., Fabian A.C. & Rees M.J., 1991, *Nature*, 350, 685
- Begelman M.C., Blandford R.D., Rees M.J., 1984, *Rev. Mod. Phys.*, 56, 255
- Begelman M.C., Cioffi D.F., 1989, *ApJ*, 345, L21
- Carilli C., Perley R.A., Dreher J.H., Leahy J.P., 1991, *ApJ*, 383, 554
- Condon J.J., Cotton W.D., Greisen E.W., Yin Q.F., Perley R.A., Taylor G.B., Broderick J.J., 1998, *AJ*, 115, 1693
- Fanaroff B.L., Riley J.M., 1974, *MNRAS*, 167, 31
- Fernini L., Burns J.O., Perley R.A., 1997, *AJ*, 114, 2292
- Gregorini L., Klein U., Parma P., Wielebinski R., Schlickeiser R., 1992, *A&AS*, 94, 13
- Ishwara-Chandra C.H., Saikia D.J., 1999, *MNRAS*, 309, 100
- Jaffe W.J., Perola G.C., 1973, *A&A*, 26, 423
- Kaiser C.R., Alexander P., 1997, *MNRAS*, 286, 215
- Kardashev, N.S., 1962, *AJ*, 6, 317
- Killeen N.E.B., Bicknell G.V., Ekers R.D., 1986, *ApJ*, 302, 306
- Klein U., Mack K.-H., 1995, *Proceedings Workshop on "Multi-Feed Systems for Radio Telescopes"*, Tucson, Ed. D.T. Emerson, ASP Conference Series
- Lacy M., Rawlings S., Saunders R., Warner P.J., 1993, *MNRAS*, 264, 721
- Lara L., Márquez I., Cotton W.D., Feretti L., Giovannini G., Marcaide J.M., Venturi T., 1999, *NewAR*, 43, 643
- Loken C., Burns D.O., Clarke D.A., Norman M.L., 1992, *ApJ*, 392, 54
- Mack K.-H., Kerp J., Klein U., 1997a, *A&A*, 324, 870
- Mack K.-H., Klein U., O'Dea C.P., Willis A.G., 1997b, *A&A*, 123, 423
- Meisenheimer K., Röser H.-J., Hiltner P.R., Yates M.G., Longair M.S., Chini R., Perley R.A., 1989, *A&A*, 219, 63
- Miley G., 1980, *ARA&A*, 18, 165
- Nath B.B., 1995, *MNRAS*, 274, 208
- Pacholczyk, A.G., 1970, *Radio Astrophysics* (San Francisco: Freeman)
- Parma P., de Ruiter H.R., Mack K.-H., van Breugel W., Dey A., Fanti R., Klein U., 1996, *A&A*, 311, 49
- Rees N., 1990, *MNRAS*, 244, 233
- Simard-Normandin M., Kronberg P.P., 1980, *ApJ*, 242, 74
- Rengelink R., Tang Y., de Bruyn A.G., Miley G.K., Bremer M.N., Röttgering H.J.A., Bremer M.A.R., 1997, *A&AS*, 124, 259
- Scheuer P.A.G., 1982, in Heeschen D.S., Wade C.M. eds, *Proc. IAU Symp. 97, "Extragalactic Radio Sources"*. Reidel, Dordrecht, p.163
- Schoenmakers A.P., de Bruyn A.G., Röttgering H.J.A., van der Laan H., 2000a, *A&A*, in preparation
- Schoenmakers A.P., Mack K.-H., de Bruyn A.G., Röttgering H.J.A., Klein U., van der Laan H., 2000b, *A&A*, in press
- Subrahmanyam R., Saripalli L., 1993, *MNRAS*, 260, 908
- Subrahmanyam R., Saripalli L., Hunstead R.W., 1996, *MNRAS*, 279, 257
- Wardle J.F.C., Kronberg P.P., 1974, *ApJ*, 194, 249
- Wieringa M., 1991, PhD. Thesis, Univ. Leiden
- Willis A.G., O'Dea C.P., 1990, in "Galactic and Intergalactic Magnetic Fields" IAU Symp. 140, Beck R., Kronberg P.P. & Wielebinski R. (eds.), Reidel, Dordrecht, p.455